Vacuum 147 (2018) 58–64

Contents lists available at ScienceDirect

Vacuum

journal homepage: www.elsevier.com/locate/vacuum

RF bias to suppress post-oxidation of μc-Si:H films deposited by inductively-coupled plasma using a planar RF resonant antenna

P. Demolon [a], Ph. Guittienne [b], A.A. Howling [a, *], S. Jost [c], R. Jacquier [a], I. Furno [a]

[a] Ecole Polytechnique Fédérale de Lausanne, Swiss Plasma Center, CH-1015 Lausanne, Switzerland
[b] Helyssen, Route de la Louche 31, CH-1092 Belmont-sur-Lausanne, Switzerland
[c] Partana 3, CH-9478 Azmoos, Switzerland

ARTICLE INFO

Article history:
Received 28 March 2017
Received in revised form
11 October 2017
Accepted 14 October 2017
Available online 16 October 2017

Keywords:
Microcrystalline silicon
Inductively-coupled plasma
RF bias
Resonant antenna
Post-oxidation

ABSTRACT

One challenge for microcrystalline silicon (μc-Si:H) deposition is to achieve high deposition rates while maintaining high quality films. In this work, an inductively-coupled plasma (ICP) is used to deposit μc-Si:H on glass substrates by means of a novel planar resonant antenna at 13.56 MHz. No particle formation occurs in the low pressure (5 Pa) plasma, but the films suffer post-oxidation. By embedding a 5 MHz RF-biased substrate, films deposited simultaneously with and without RF bias are compared. It is shown that large area, low pressure (5 Pa), particle-free ICP deposition at 1 nm/s of μc-Si:H films can be obtained without post-oxidation by means of a planar resonant antenna, provided that RF substrate bias is included for independent control of the ion energy.

1. Introduction

Hydrogenated microcrystalline silicon (μc-Si:H) thin films have found widespread application, for example, in flat panel display and solar cell industries [1–6]. Plasma-enhanced chemical vapor deposition has been used for large area (>1 m^2) deposition of μc-Si:H by using capacitively-coupled plasma (CCP) reactors [3,4,7]. One drawback of CCP at the conventional 13.56 MHz frequency is the limitation of the deposition rate to obtain high material quality [8]. A related problem is the high ion bombardment energy onto the growing film due to the high voltage RF sheaths (typically, 10^2 V) which can lead to an accumulation of stress with a risk of post-process delamination or degradation of the film electrical properties. Various techniques have been successful for reducing ion energy for high quality μc-Si:H deposition in CCP, such as Very High Frequency [4,8–13], and special reactor configurations [14–16]. Also, collisional sheaths [9,11,12,16–18] can reduce the ion energy at the substrate because ions lose energy while crossing the sheath potential. For this to occur, the ion mean free path must be short (~10^{-1} mm) compared to the sheath width (~10^{0} mm). This requires high pressures, ~10^{0} mbar (~10^2 Pa), which can lead to radical agglomeration and powder formation, deleterious for plasma processing [19].

Inductively-coupled plasma (ICP) has also been used to deposit μc-Si:H on glass because the high plasma density can yield fast deposition rates [20–26], and large area ICP reactors have been developed for this purpose [5,21,24,27–41]. Furthermore, ICPs are characterized by low sheath voltages: The minimum ion energy, ~20 eV, for ICPs is determined by the floating sheath potential drop (~20 V) which is much lower than for conventional CCP where the ion bombardment energy can be of the order of 10^2 eV [6,27]. However, if μc-Si:H films exhibit post-oxidation, whether deposited by ICP or low-ion-energy CCP, this is incompatible with high quality material [26,42,43]. One conclusion has been that at least some moderate ion bombardment energy (more than 20 eV but less than 10^2 eV, depending on the reactor and plasma parameters) is necessary to produce high quality films [44–49].

In this paper we show the first results obtained for μc-Si:H deposition using a novel, large area, 13.56 MHz planar resonant antenna as an ICP source [41]. This network could be considered as an alternative to coil ICPs by providing a spatially-distributed resonance structure over the whole plasma area [41,50]. After describing the experimental setup in Section 2, the deposited layers without RF bias (Section 3.1) and with RF bias (Section 3.2) are compared in terms of post-oxidation, by embedding a 5 MHz RF-

* Corresponding author.
E-mail address: alan.howling@epfl.ch (A.A. Howling).

https://doi.org/10.1016/j.vacuum.2017.10.020
0042-207X/

biased substrate. The effects of RF bias on μc-Si:H deposition are discussed in Section 4. It is concluded that large area, low pressure (5 Pa), particle-free ICP deposition of μc-Si:H films without post-oxidation can be obtained using a RF resonant antenna, provided that RF substrate bias is included for independent control of ion energy.

2. Experiment description

The planar RF resonant antenna source in Fig. 1 is made up of 23 parallel copper legs 37 cm long, regularly spaced to define a 47 × 37 cm^2 plasma area. The legs, which act as inductors, are interconnected at both ends by 1.1 nF capacitors. With this design, the antenna network presents a mode resonance at 13.56 MHz [50]. This concept of spatially-distributed mode resonance has been demonstrated for ICP plasmas as large as 1.4 m^2 [41], and can in principle be extended to indefinitely-large areas. The resulting antenna resonance currents generate RF plasma currents by magnetic induction, without the need for currents across the capacitive sheaths, and hence the sheath voltage can be as low as the floating potential (~20 V). The 13.56 MHz RF power (typically 1 kW) for the ICP resonant antenna was connected to one end of the central leg, and the antenna current returned via two neighboring connectors to the grounded housing, as shown in Fig. 1. The entire antenna assembly is embedded in polyimide dielectric foam to prevent spurious plasma ignition within the antenna. The lower surface of this foam is protected from plasma exposure by a set of 12 overlapping alumina tiles, 0.5 mm thick, mounted using ceramic screws.

The grounded, aluminum reactor housing encloses the whole assembly and forms the ground reference for the 13.56 MHz antenna and also for a 5 MHz RF bias supply (described below). The reactor is placed inside a vacuum chamber.

The films were deposited on a glass substrate placed on the aluminum baseplate 7 cm below the alumina tiles. Silicon wafer samples, placed on the glass, were used for characterization by Raman and Fourier Transform Infrared (FTIR) spectroscopy. The substrate was heated to 220 °C by means of resistive heating wire outside the reactor. The pressure for all the depositions was 5 Pa; at this low pressure, no powder was observed in the reactor nor in the exhaust, which is an advantage of this ICP deposition method, in contrast to CCP at mbar (10^2 Pa) pressures [19]. Thus ICP can avoid particulate contamination of the growing film, as well as costly downtime for reactor and exhaust cleaning, and pump maintenance. The flowrates for silane and hydrogen were respectively 20–100 sccm and 250–750 sccm, depending on the dilution and the required deposition rate.

Control of the ion bombardment energy was achieved by incorporating an independent 10 × 10 cm^2 RF biased plate in the center of the base of the grounded housing as shown in Fig. 1(b). A 5 MHz RF generator of 50 W maximum power was used to apply a peak-to-peak voltage of up to 250 V_{pp} on this plate, referenced to the grounded housing. Because the RF bias voltage is directly applied between the bias plate and ground, it is a CCP source, where the RF voltage appears across the series impedance of the plasma and the sheaths. Because the sheath capacitive impedance varies inversely with frequency, frequencies of a few MHz or less ensure that the principal voltage drop occurs across the sheaths, which is the aim of the RF bias to control the ion energy. 5 MHz was sufficiently far below 13.56 MHz so that simple filters could be used to suppress any interference between the power supply circuits, although other frequencies could be used. Simultaneous comparison of depositions with and without RF bias was made between silicon wafer samples located inside and outside of the bias area. The deposition conditions are summarized in Table 1 in the

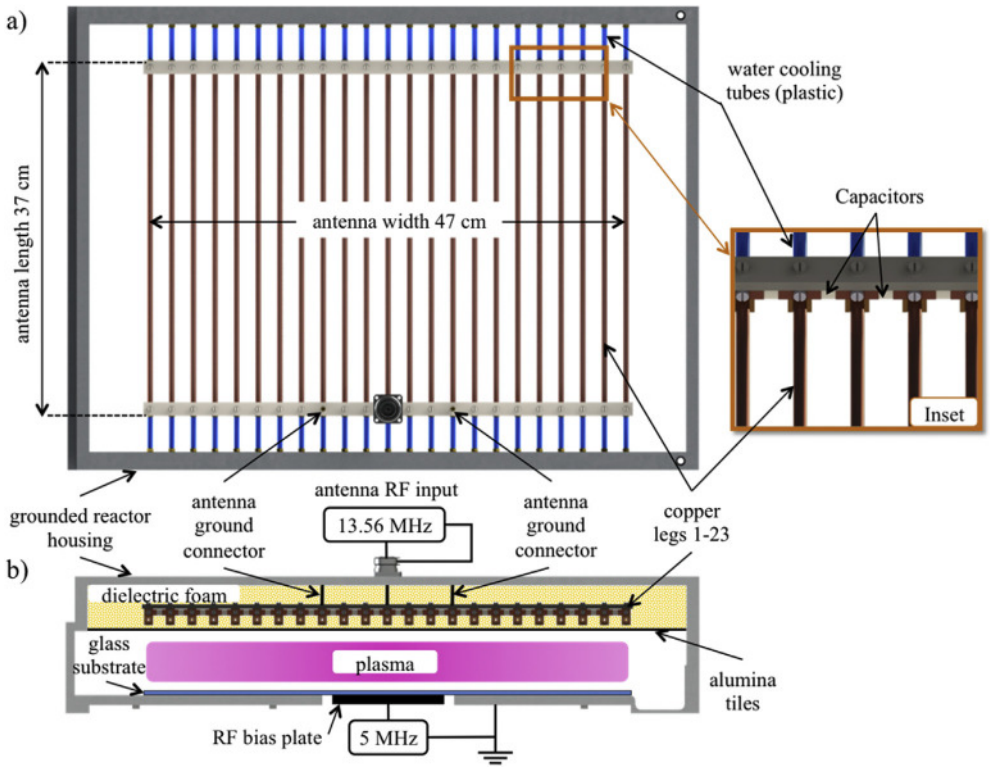

Fig. 1. Scale drawings of the novel ICP reactor: (a) Open plan view showing the planar RF antenna; the inset shows the capacitors, copper legs, and the cooling tubes. (b) Cross-section of the reactor showing the 13.56 MHz RF power (1 kW) input to the antenna, and the 5 MHz RF bias plate supply (50 W). The antenna is embedded in dielectric foam and protected by alumina tiles. The glass substrate with silicon wafer samples rests on the grounded baseplate and the RF bias plate.

appendix.

The film crystallinity was measured by means of Raman spectroscopy (532 nm laser and 0.25 cm^{-1} resolution) by spectral deconvolution of three Gaussian functions centered at the 480, 510 and 520 cm^{-1} peaks [51–53]. Post-oxidation of the films was measured using FTIR spectroscopy (400 - 4000 cm^{-1} with 2 cm^{-1} resolution) using the peak identification of Bronneberg et al. [54], as described in section 3.1. The film refractive index, measured at 500 nm by spectroscopic ellipsometry, was analyzed according to the effective medium technique [55,56] as described in section 3.2.

3. Results

The properties of films deposited by the planar ICP source without RF bias are shown in Section 3.1 in order to provide the reference conditions. The effect on post-oxidation of the film by adding RF bias at 5 MHz is then described in Section 3.2.

3.1. μc-Si:H films deposited without RF bias

Fig. 2(a) shows Raman measurements for samples deposited with different H_2 dilutions at the same deposition rate. As shown by previous studies [57], stronger hydrogen dilution clearly increases the crystallinity. In Fig. 2(b), the Raman spectra with 90% H_2 dilution reveal that crystalline fractions of about 65%, corresponding to the requirements for PV quality μc-Si:H layers [7,12,58,59], can be obtained regardless of the deposition rate. Hence 90% H_2 dilution was used as the reference condition for all subsequent depositions. These results show that the films deposited by the planar resonant antenna have a similar crystallinity dependence, regarding hydrogen dilution, to those of other plasma deposition reactors [57].

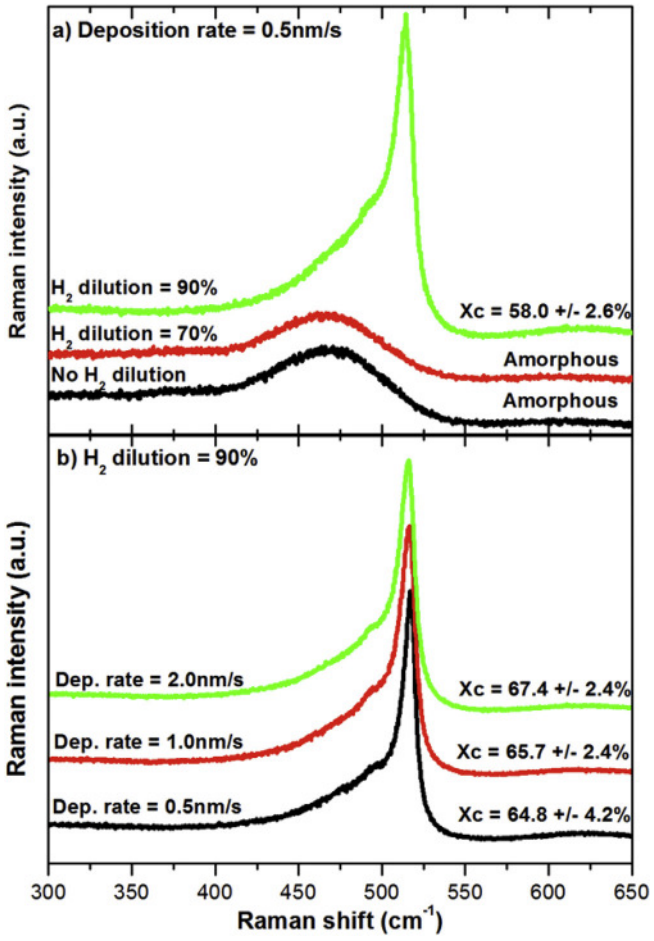

Fig. 2. Raman spectroscopy measurements and crystallinity results Xc as a function of Raman shift, without RF bias; (a) for various H_2 dilutions at a constant deposition rate of 0.5 nm/s, by varying the silane and hydrogen flowrates, and (b) for various deposition rates at constant 90% H_2 dilution, also by varying the silane and hydrogen flowrates. The RF power at 13.56 MHz was fixed at 1 kW, and the pressure was fixed at 5 Pa. The spectra are displaced vertically for clarity.

Fig. 3 shows FTIR spectra of a film measured for different times after deposition. Characteristic absorption regions for a μc-Si:H sample [54,60] include the Si-H_x wagging at 600-700 cm^{-1}, Si-H_2 bending at 850-910 cm^{-1}, and Si-H_x stretching at 2000-2150 cm^{-1}. Amongst the Si-H_x stretching modes, the low stretching mode (LSM) near 2000 cm^{-1} and the broad high stretching mode (HSM) around 2100 cm^{-1} have been described in the literature [60]. These peaks and their intensities give some indication about the oxidation of the μc-Si:H layer, as follows:

(i) In Fig. 3, the spectrum measured 10 min after deposition already shows a significant Si-O-Si asymmetric stretching peak at 1000 - 1200 cm^{-1} corresponding to oxygen contamination which is incompatible with the electrical properties required for device-grade material [11,26,42,43,60]. This is probably due to residual oxygen contamination from gas lines and outgassing of the dielectric foam in this prototype reactor [61], as well as from exposure to air after venting the vacuum chamber. For the spectra at later times, the amplitude of the Si-O-Si peak (as well as the O_xSiH_y peak) strongly increases, while the intensities of the SiH_x stretching and wagging are reduced: The μc-Si:H structure has changed by promoting the strong Si-O-Si bonds, as demonstrated by Bronneberg et al. [54].

(ii) The LSM (~2000 cm^{-1}) is almost absent in all of the spectra in Fig. 3, while the HSM (~2100 cm^{-1}) dominates. Bronneberg et al. [54] have proposed that this behavior reveals that the amorphous tissue between the grains has nanovoids. Fig. 3 shows the HSM of the amorphous tissue diminishing as the film oxidizes [54].

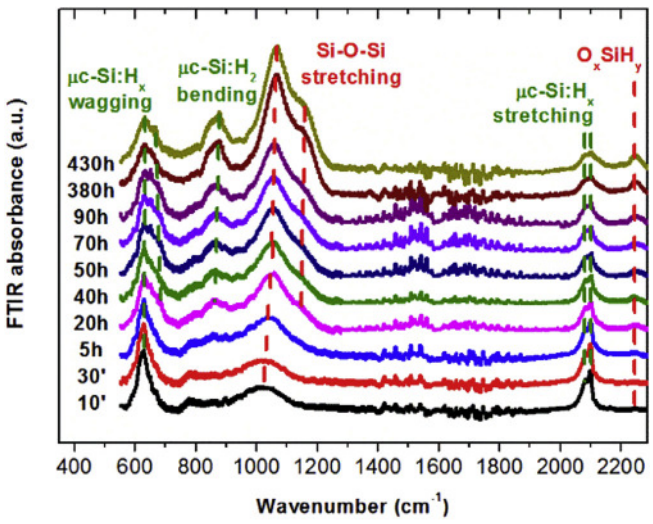

Fig. 3. Time dependence of FTIR spectra after deposition, without RF bias, of a μc-Si:H film deposited at 1.9 nm/s. The H_2 and SiH_4 flows were respectively 650 and 70 sccm (90% H_2 dilution). 13.56 MHz RF power at 1 kW and 5 Pa pressure. The spectra are displaced vertically for clarity.

Post-oxidation of Si films is deleterious for solar cell performance [43,60]. The use of high H_2 dilution exacerbates this effect due to the formation of Si-H bonds in the crystalline grain boundaries, where contact with air promotes the formation of SiO_x and O_xSiH_y bonds [54].

Fig. 4 shows the continuing post-oxidation [26] by plotting the increase with time of the area of the FTIR peak for SiO_x (1000-1200 cm^{-1}), divided by its initial area. The amount of post-oxidation is clearly greater for films deposited at faster deposition rates.

3.2. Effect of the RF bias on post oxidation of the μc-Si:H film

To illustrate the effect of ion bombardment on post oxidation, Fig. 5 shows the FTIR spectra obtained for two samples deposited simultaneously in the same process, one located inside the RF bias region (see Fig. 1(b)), and the other outside. Raman measurements show a crystallinity of 63–65% for both samples (not shown). For this example, the applied RF bias voltage was $V_{pp} = 200$ V at 5 MHz. The deposition rate was 0.88 nm/s for the sample inside the bias zone, and 0.7 nm/s for the sample outside the bias zone. This shows that the RF bias was not strongly affecting the plasma deposition rate because this non-uniformity is consistent with the dome shape typically measured for large area planar resonant antenna sources [41]. Furthermore, the RF bias 5 MHz power supply was limited to 50 W maximum power, which is less than 5% of the ICP antenna power of 1 kW at 13.56 MHz. This confirms that the 5 MHz bias power supply does not strongly perturb the power dissipated in the plasma by the ICP antenna. The ion bombardment energy caused by the RF bias was not measured directly, but for such an asymmetric arrangement (bias electrode area ≪ total grounded area), an upper limit for the ion energy would be given by $eV_{pp}/2 = 100$ eV [62]. Furthermore, this ion energy is gained by crossing the voltage drop of the sheath in front of the smaller electrode [62], that is to say, at the RF bias electrode in this case. To summarize, the action of the 50 W RF bias supply at 5 MHz is principally to provide a negative polarization DC bias at the RF bias electrode, whereas the 1 kW ICP at 13.56 MHz supplies the dissipated power responsible for plasma dissociation and deposition.

Fig. 5(a) shows that the FTIR spectra of both samples measured just after deposition are similar. However, after 800 h, Fig. 5(b) shows a very clear effect of the RF bias:

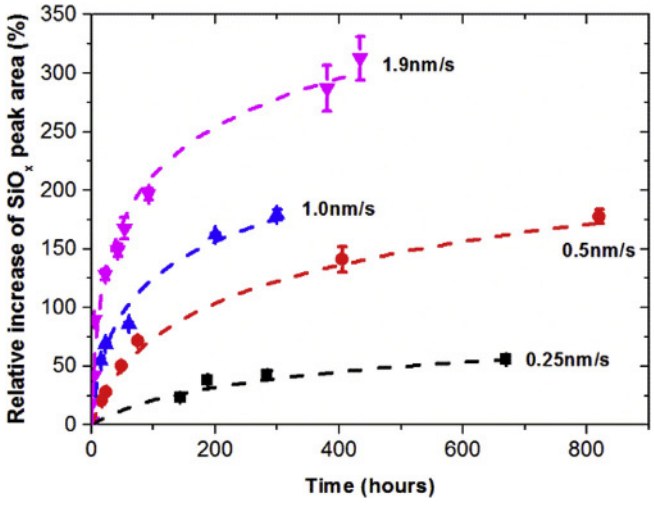

Fig. 4. Relative increase in the SiO_x peak (1000-1200 cm^{-1}) with time after deposition, without RF bias, for different deposition rates (labelled for each line) with 90% H_2 dilution. The dashed lines are drawn to guide the eye.

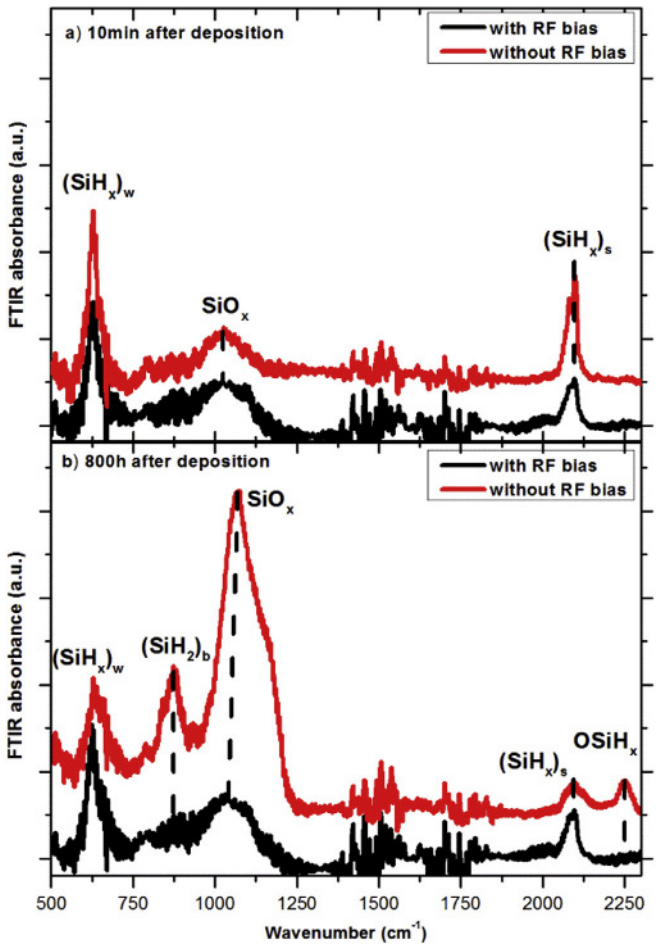

Fig. 5. Comparison of the FTIR spectra with (black line) and without (red line) RF bias (200 V_{pp} at 5 MHz) (a) 10 min after deposition, and (b) after 800 h. The H_2 dilution was 90% at 5 Pa pressure and the ICP antenna RF power was 1 kW at 13.56 MHz. The spectra are displaced vertically for clarity. (For interpretation of the references to colour in this figure legend, the reader is referred to the web version of this article.)

(i) The FTIR spectrum of the sample without RF bias shows a strong increase in the Si-O-Si and O_xSiH_y peaks, whereas the spectrum for the sample deposited with RF bias remains unchanged even after 800 h. This is the main result of this paper, and it clearly shows that the substrate RF bias can be used to avoid post-oxidation in the growing μc-Si layers [44–49,60].

(ii) The HSM (~2100 cm^{-1}) dominates the LSM (~2000 cm^{-1}) for all cases, as also in Fig. 3, indicating that the amorphous tissue exhibits nanovoids, according to Ref. [54]. For the unbiased samples, the HSM diminishes as the amorphous tissue oxidizes [54], also as in Fig. 3. However, for the RF-biased material, the HSM remains unchanged by exposure to air; this could be interpreted as though the amorphous tissue were sealed within the film, thus protecting both the micro-crystalline and the amorphous phases from post-oxidation.

Both (i) and (ii) are consistent with the interpretation that ion bombardment due to the RF bias results in films resistant to post-oxidation [48].

Fig. 6 illustrates the influence of the RF bias peak-to-peak voltage on the layer post-oxidation for different deposition rates. The post-oxidation of each film is characterized here by the relative

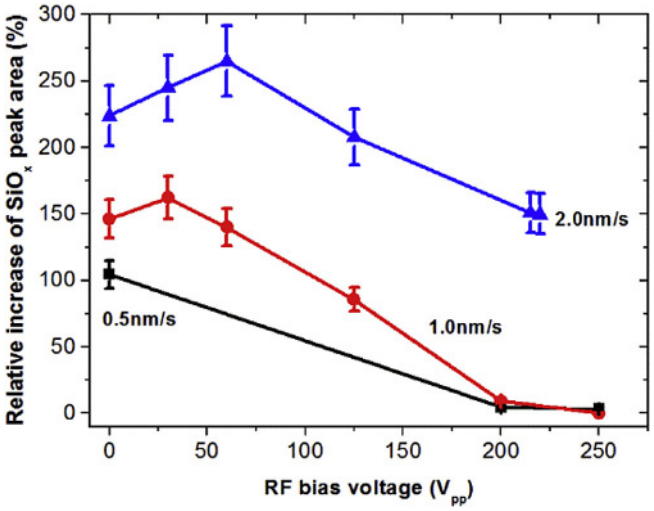

Fig. 6. Relative increase in the SiO_x peak (1000-1200 cm^{-1}) one week after the depositions, as a function of the RF bias peak-to-peak voltage at 5 MHz, for three deposition rates (labelled on the lines) by varying the silane and hydrogen flowrates. The hydrogen dilution was 90% at 5 Pa pressure, and the ICP antenna RF power was 1 kW at 13.56 MHz.

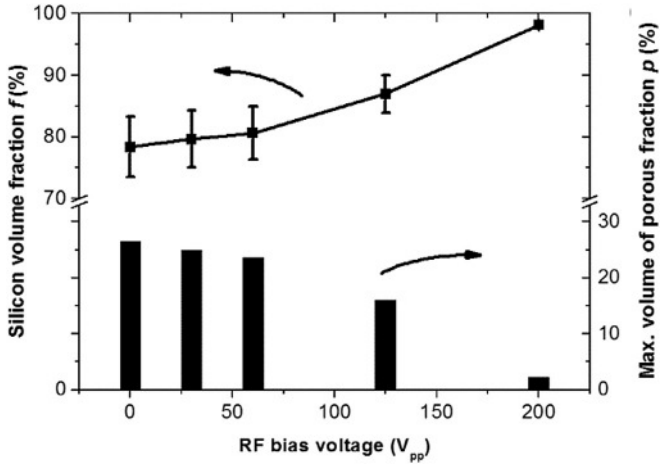

Fig. 7. Using refractive index measurements to estimate the initial volume fraction of silicon (line) and the maximum fraction of pores in the layer (bars), as a function of the RF bias voltage at 5 MHz, for a deposition rate of 1 nm/s with 90% H_2 dilution. The ICP antenna RF power was 1 kW at 13.56 MHz, with 5 Pa pressure.

increase of the Si-O-Si peak after one week. For growth rates up to 1 nm/s, a 200 V_{pp} RF bias is sufficient to avoid post-oxidation. For higher rates, the same trend is observed, but higher voltages should probably be applied to suppress post-oxidation, unless the ion energy becomes so high that ion bombardment damage occurs [44].

Films of μc-Si:H were also investigated by measuring their refractive index which can be interpreted using the Bruggeman Effective Medium Approximation [56]. Using the technique of Astrova and Tolmachev [55], the volume fractions of the film are deduced by making some assumptions based on the known properties of silicon and silicon oxide, for example, that oxidation of silicon produces a factor 2.27 increase in volume [55]. In this way, the silicon volume fraction and the volume of porous fraction can be estimated: If f is the silicon volume fraction before oxidation, and x is the part of silicon converted to silicon oxide occupying a volume $2.27x$, then the post-oxidized layer is composed of volume fractions $(f - x)$ of silicon, and $2.27x$ of silicon oxide. Therefore, the volume of porous fraction, p, is $p = 1 - (f - x) - 2{:}27x = 1 - f - 1{:}27x$. Using these volume fractions, the Bruggeman effective medium equation [55]

$$(f - x)F + 2{:}27xG + pV = 0; \quad (1)$$

gives the relation between the material refractives indexes and their volume fractions. The parameters F, G, V are given by

$$F = \frac{n_{Si}^2 - n^2}{n_{Si}^2 + 2n^2};$$
$$G = \frac{n_{SiO_2}^2 - n^2}{n_{SiO_2}^2 + 2n^2};$$
$$V = \frac{1 - n^2}{1 + 2n^2};$$

where n_{Si}; n_{SiO_2} are the refractive indexes of silicon and silicon oxide respectively, and n is the index of the post-oxidized film measured by spectroscopic ellipsometry.

Fig. 7 shows the estimated range of the initial volume fraction of silicon, f, and the maximum value for the porous volume fraction p, as a function of RF bias voltage. These results were obtained on samples deposited at 1 nm/s; similar trends were observed for 0.5 and 2 nm/s. The effect of the RF bias is to increase the silicon volume fraction to about 98% for a RF peak-to-peak bias voltage of 200 V_{pp}.

4. Discussion of the effect of RF bias on μc-Si:H thin film deposition

In this section, possible explanations for the experimental observations are considered, in order of increasing ion bombardment energy.

4.1. Film growth with no RF bias (floating potential, ion energy < 20 eV)

It is generally observed that ICP deposition of μc-Si:H at low substrate temperature (T_{sub} ~ 100–300 °C) without RF bias results in films consisting of columnar structures with a rough surface [26]. The silicon nanostructures oxidize gradually and uniformly throughout the film thickness when exposed to air which diffuses into the surfaces of the cracks between the columns during days and weeks at room temperature. This post-oxidation is responsible for poor electrical properties [63,64].

To explain this columnar growth, we note that the substrate temperature, T_{sub}, is much less than the film melting temperature T_{melt} ~1200–1400 °C, for which T_{sub}=T_{melt} < 0:25 in Kelvin; this means that the films are synthesised far from thermodynamic equilibrium [65]. By analogy with physical vapor deposition (PVD), this low ratio corresponds to low adatom mobility where the surface atoms can move only 1 to 3 atomic positions, resulting in deposition of columnar thin films with vertical cracks running through the film thickness, and an underdense morphology. Columns preserve the random orientation of nucleation sites as predicted by ballistic models, and surface roughness causes atomic shadowing leading to columnar growth in the presence of limited surface diffusion [65], especially on substrates with sharp-edged roughness [43]. This mechanism is consistent with the PVD-like deposition of μc-Si:H by SiH_2 radicals in diluted silane plasmas [66,67]. Competition between surface mobility and growth rate means that faster-deposited films are more susceptible to post oxidation [43,63], consistent with the results shown in Fig. 4.

4.2. Film growth using moderate RF bias (ion energy ~ 30–60 eV)

Low energy ion irradiation during growth is extensively used to overcome rough and underdense microstructures of refractory materials deposited at low substrate temperature (typically T_{sub}=T_{melt} < 0:25) [65]. In structure zone models [68,69], the concurrent ion bombardment energy per adatom, inherent in plasma-enhanced CVD, provides an additional dimension for modifying the thin film microstructure. The ions contribute a hyperthermal surface-localized energy, which enhances surface mobility beyond the values associated with T_{sub}=T_{melt} < 0:25 [65]. For ion energies >20 eV, ions can also displace a Si atom at the surface, which directly enhances surface migration and is characterized by a reduction in nanovoids and an improvement in electrical properties. This ion-bombardment-induced adatom mobility can eliminate shadowing effects and redistribute materials between clusters and columns, which transforms the microstructure into a transition zone material with compressive stress, a smoother surface, and a film with only short-range (<10 nm) void distributions that do not traverse the film thickness [68]. These films therefore do not absorb atmospheric oxygen. The competition between enhanced surface mobility (depending on ion flux and energy) and growth rate (depending on adatom flux) means that faster-deposited films require higher-voltage RF biasing to resist post oxidation, consistent with results shown in Fig. 6. For these airtight films, the initial oxygen content in Fig. 5(a) is assumed to come from reactor outgassing during plasma deposition.

RF biasing has also been used to manipulate the microstructure of μc-Si:H in a remote expanding thermal plasma [70] and in magnetron sputtered films [71], where −40 V DC bias was sufficient to increase the surface mobility of the radicals, without damaging the structure. Analogous observations were also made using silicon transport in a DC hydrogen plasma [72]: Post-oxidation occurred for films deposited at floating potential, whereas no oxygen incorporation was observed for films deposited with a DC bias of −50 V.

4.3. Film damage using high RF bias (ion energy > 60 eV)

For ion energies above 60 eV, high defect densities and compressive stress can occur [65]. Ions can displace a Si atom in the bulk (several mono-layers deep) causing local amorphization of the μc-Si:H film and incorporation of vacancies [16,18,70]. In magnetron sputtering deposition, this degrades crystallinity by breaking ordered Si-Si bonds [71].

In conclusion, plasma deposition of μc-Si:H films is a physico-chemical process, whereby plasma-enhanced CVD provides the SiH_x and H radicals, and ion energy provides the PVD-enhanced surface mobility to avoid columnar growth. Films with good electrical properties can only be obtained by careful compromise of growth rate, substrate temperature, ion energy and ion flux [65]. The experimental observations in Figs. 4 and 6 are consistent with this model. Ideally, the ion energies and fluxes should all be adapted throughout film growth [44]. In CCP sources, the sheath voltage depends on the discharge power, whereas RF bias provides independent control of ion energy in the planar resonant ICP source.

5. Conclusions

Hydrogenated microcrystalline silicon (μc-Si:H) thin films were deposited using a 13.56 MHz inductively-coupled plasma generated by a novel planar resonant antenna in silane with 90% hydrogen dilution. This resonant network concept could be considered as an alternative to coil ICPs by providing a spatially-distributed mode resonance structure over the whole plasma area [41]. However, without RF bias, the deposited layers suffered strong post-oxidation even for low deposition rates of about 0.2 nm/s. By applying a 5 MHz RF bias voltage to an embedded substrate during deposition, the post-oxidation of the μc-Si:H layers was reduced: For deposition rates up to 1 nm/s, using 200 V peak-to-peak voltage for a maximum ion energy of ~100 eV, post-oxidation was eliminated. Enhanced surface mobility, due to ion impact and localized hyperthermal heating, is the probable factor in the reduction of columnar structures and post-oxidation of plasma-deposited μc-Si:H.

The combined use of an ICP source with substrate RF bias is advantageous because the ion bombardment energy can be chosen independently of the RF power of the ICP to optimize the layer properties, in contrast to CCP reactors where the ion bombardment energy depends on the source power.

In conclusion, it is shown that ICP deposition of μc-Si:H films resistant to post-oxidation can be obtained using a planar resonant antenna, provided that RF substrate bias is included for independent control of ion energy.

Acknowledgments

This work was supported by Swiss Commission for Technology and Innovation grant no. 15082.1 PFIW-IW, and TEL Solar AG, Switzerland.

Appendix

Table 1
Summary of the deposition conditions for Figs. 2–6. Deposition rate R [nm/s], dilution of the silane flow as a percentage of the total flow, RF bias voltage as a peak-to-peak voltage, and Raman crystallinity percentage X_c. For all depositions: film thickness is 1 ± 0.2 μm, total pressure 5 Pa, substrate temperature 220 °C, RF power 1 kW at 13.56 MHz, RF bias at 5 MHz.

Fig. No.	R [nm/s]	Dilution [%]	Bias voltage [V_{pp}]	X_c [%]
Fig. 2(a)	0.5	0, 70	0	0
	0.5	90	0	58.0 ± 2.6
Fig. 2(b)	0.5	90	0	64.8 ± 4.2
	1	90	0	65.7 ± 2.4
	2	90	0	67.4 ± 2.4
Fig. 3	1.9	90	0	~65
Fig. 4	0.25,0.5,1,1.9	90	0	~65
Fig. 5	0.7	90	0	~65
	0.88	90	200	~65
Fig. 6	0.5	90	0,200,250	~65
	1	90	0,30,60,125,200,250	~65
	2	90	0,30,60,125,215,220	~65

References

[1] J. Meier, R. Flückiger, H. Keppner, A. Shah, Appl. Phys. Lett. 65 (1994) 860.
[2] J. Meier, S. Dubail, S. Golay, U. Kroll, S. Faÿ, E. Vallat-Sauvain, L. Feitknecht, J. Dubail, A. Shah, Sol. Energy Mater. Sol. Cells 74 (2002) 457.
[3] A. Terakawa, Sol. Energy Mater. Sol. Cells 119 (2013) 204.
[4] H. Takatsuka, M. Noda, Y. Yonekura, Y. Takeuchi, Y. Yamauchi, Sol. Energy 77 (2004) 951.
[5] T. Takagi, M. Ueda, N. Ito, Y. Watabe, H. Sato, K. Sawaya, Thin Solid Films 502 (2006) 50.
[6] S.Q. Xiao, S. Xu, K. Ostrikov, Mater. Sci. Eng. R. Rep. 78 (2014) 1.
[7] C. Ellert, C. Wachtendorf, A. Hedler, M. Klindworth, M. Martinek, Sol. Energy Mater. Sol. Cells 96 (2012) 71.
[8] U. Kroll, J. Meier, P. Torres, J. Pohl, A. Shah, J. Non-Cryst. Solids 227–230 (1998) 68.
[9] A.H.M. Smets, T. Matsui, M. Kondo, J. Appl. Phys. 104 (2008) 034508.
[10] C. Strobel, B. Leszczynska, U. Merkel, J. Kuske, D.D. Fischer, M. Albert, J. Holovský, S. Michard, J.W. Bartha, Sol. Energy Mater. Sol. Cells 143 (2015) 347.

[11] T. Matsui, A. Matsuda, M. Kondo, Sol. Energy Mater. Sol. Cells 90 (2006) 3199.
[12] Y. Mai, S. Klein, R. Carius, J. Wolff, A. Lambertz, F. Finger, X. Geng, J. Appl. Phys. 97 (2005) 114913.
[13] M. Heintze, R. Zedlitz, J. Non-Cryst. Solids 198–200 (1996) 1038.
[14] M. Chesaux, A.A. Howling, C. Hollenstein, D. Dominé, U. Kroll, J. Vac. Sci. Technol. A31 (2013) 021302.
[15] C. Niikura, M. Kondo, A. Matsuda, J. Non-Cryst. Solids 388–340 (2004) 42.
[16] T. Matsui, A. Bidiville, K. Maejima, H. Sai, T. Koida, T. Suezaki, M. Matsumoto, K. Saito, I. Yoshida, M. Kondo, Appl. Phys. Lett. 106 (2015) 053901.
[17] L. Guo, M. Kondo, M. Fukawa, K. Saitoh, A. Matsuda, Jpn. J. Appl. Phys. 37 (1998) L1116.
[18] M. Kondo, M. Fukawa, L. Guo, A. Matsuda, J. Non-Cryst. Solids 266–269 (2000) 84.
[19] B. Strahm, C. Hollenstein, J. Appl. Phys. 107 (2010) 023302.
[20] S.Q. Xiao, S. Xu, D.Y. Wei, S.Y. Huang, H.P. Zhou, Y. Xu, J. Appl. Phys. 108 (2010) 113520.
[21] D.Y. Wei, S.Q. Xiao, S.Y. Huang, C.S. Chan, H.P. Zhou, L.X. Xu, Y.N. Guo, J.W. Chai, S.J. Wang, S. Xu, J. Phys. D. Appl. Phys. 46 (2013) 215501.
[22] S. Won, J. Youn, J. Jang, B. Moon, Journal-Korean Phys. Soc. 39 (2001) 123.
[23] N. Kosku, S. Miyazaki, Thin Solid Films 511–512 (2006) 265.
[24] E. Takahashi, Y. Nishigami, A. Tomyo, M. Fujiwara, H. Kaki, K. Kubota, T. Hayashi, K. Ogata, A. Ebe, Y. Setsuhara, Jpn. J. Appl. Phys. 46 (2007) 1280.
[25] Q. Cheng, S. Xu, S. Huang, K.K. Ostrikov, Cryst. Growth Des. 9 (2009) 2863.
[26] G. Nogay, E. Özkol, S. Ilday, R. Turan, Vacuum 110 (2014) 114.
[27] Y. Setsuhara, K. Takenaka, A. Ebe, K. Nishisaka, Solid State Phenom. 127 (2007) 239.
[28] Z. Yu, D. Shaw, P. Gonzales, G.J. Collins, J. Vac. Sci. Technol. A 13 (1995) 871.
[29] Y. Wu, M.A. Lieberman, Appl. Phys. Lett. 72 (1998) 777.
[30] S.E. Park, B.U. Cho, J.K. Lee, Y.J. Lee, G.Y. Yeom, IEEE Trans. Plasma Sci. 31 (2003) 628.
[31] T. Meziani, P. Colpo, F. Rossi, J. Appl. Phys. 99 (2006) 033303.
[32] Y. Kawai, H. Ikegama, N. Sato, A. Matsuda, K. Uchino, M. Kuzuya, A. Mizuno (Eds.), Industrial Plasma Technology, Wiley, Weinheim, 2008.
[33] H.-S. Jun, H.-Y. Chang, Appl. Phys. Lett. 92 (2008) 041501.
[34] J.H. Lim, K.N. Kim, J.K. Park, J.T. Lim, G.Y. Yeom, Appl. Phys. Lett. 92 (2008) 051504.
[35] K.N. Kim, Y.J. Lee, S.J. Kyong, G.Y. Yeom, Surf. Coat. Technol. 177–178 (2004) 752.
[36] V.A. Godyak, Plasma Sources Sci. Technol. 20 (2011) 025004.
[37] J.-W. Lee, Y.-S. Lee, H.-Y. Chang, S.-H. An, Phys. Pl. 21 (2014) 083502.
[38] H.J. Kim, H.-J. Hwang, D.H. Kim, J.H. Cho, H.S. Chae, C.-W. Chung, J. Appl. Phys. 117 (2015) 153302.
[39] D.K. Tripathi, F. Jiang, M. Martyniuk, J. Antoszewski, K.K.M.B.D. Silva, J.M. Dell, L. Faraone, J. Microelectromech. Syst. 24 (2015) 1998.
[40] Sentech Instruments GmbH, http://www.sentech.com.
[41] P. Guittienne, R. Jacquier, A.A. Howling, I. Furno, Plasma Sources Sci. Technol. 26 (2017) 035010.
[42] G. Nogay, Z.M. Saleh, E. Özkol, R. Turan, Mater. Sci. Eng. B 196 (2015) 28.
[43] G. Bugnon, G. Parascandolo, T. Söderström, P. Cuony, M. Despeisse, S. Hänni, J. Holovsky, F. Meillaud, C. Ballif, Adv. Funct. Mater 22 (2012) 3665.
[44] B. Kalache, A.I. Kosarev, R. Vanderhaghen, P. Roca i Cabarrocas, J. Appl. Phys. 93 (2003) 1262.
[45] M. Chesaux, A Grid Reactor with Low Ion Bombardment Energy for Large Area PECVD of Thin Film Silicon Solar Cells, PhD Thesis no. 5686, 2013, https://doi.org/10.5075/epfl-thesis-5686. Lausanne, Switzerland.
[46] N. Kosku, H. Murakami, S. Higashi, S. Miyazaki, Appl. Surf. Sci. 244 (2005) 39.
[47] X.D. Zhang, F.R. Zhang, E. Amanatides, D. Mataras, Y. Zhao, Thin Solid Films 516 (2008) 6912.
[48] A.C. Bronneberg, M.C.M. van de Sanden, M. Creatore, J. Non-Cryst. Solids 358 (2012) 379.
[49] V.L. Dalal, J. Graves, J. Leib, Appl. Phys. Lett. 85 (2004) 1413.
[50] P. Guittienne, A.A. Howling, C. Hollenstein, Plasma Sources Sci. Technol. 23 (2014) 015006.
[51] M. Vanacek, J. Kocka, J. Strichlik, Z. Kosicek, O. Stika, A. Triska, Sol. Energy Mater 8 (1983) 411.
[52] T. Kaneko, M. Wakagi, K. Onisawa, T. Minemura, Appl. Phys. Lett. 64 (1994) 1865.
[53] S. Veprek, F.A. Sarott, Z. Iqbal, Phys. Rev. B 36 (1987) 3344.
[54] A.C. Bronneberg, A.H.M. Smets, M. Creatore, M.C.M. van de Sanden, J. Non-Cryst. Solids 357 (2011) 884.
[55] E.V. Astrova, V.A. Tolmachev, Mater. Sci. Eng. B69–70 (2000) 142.
[56] D.A.G. Bruggeman, Ann. Phys. 24 (1935) 636.
[57] P. Alpuim, V. Chu, J.P. Conde, J. Appl. Phys. 86 (1999) 3812.
[58] O. Vetterl, F. Finger, R. Carius, P. Hapke, L. Houben, O. Kluth, A. Lambertz, A. Mück, B. Rech, H. Wagner, Sol. Energy Mater. Sol. Cells 62 (2000) 97.
[59] M.N. van den Donker, T. Kilper, D. Grunsky, B. Rech, L. Houben, W.M.M. Kessels, M.C.M. van de Sanden, Thin Solid Films 515 (2007) 7455.
[60] A.H.M. Smets, T. Matsui, M. Kondo, Appl. Phys. Lett. 92 (2008) 033506.
[61] U. Kroll, J. Meier, H. Keppner, A. Shah, S.D. Littlewood, I.E. Kelly, P. Giannoulès, J. Vac. Sci. Technol. A13 (1995) 2742.
[62] K. Köhler, J.W. Coburn, D.E. Horne, E. Kay, J.H. Keller, J. Appl. Phys. 57 (1985) 59.
[63] F. Finger, R. Carius, T. Dylla, S. Klein, S. Okur, M. Günes, J. Optoelectron. Adv. M. 7 (2005) 83.
[64] S. Vepřek, Z. Iqbal, R.O. Kühne, P. Capezzuto, F.-A. Sarott, J.K. Gimzewski, J. Phys. C. Solid State Phys. 16 (1983) 6241.
[65] I. Petrov, P.B. Barna, L. Hultman, J.E. Greene, J. Vac. Sci. Technol. A 21 (2003) S117.
[66] C.C. Tsai, J.C. Knights, G. Chang, B. Wacker, J. Appl. Phys. 59 (1986) 2998.
[67] T. Kuwahara, H. Ito, K. Kawaguchi, Y. Higuchi, N. Ozawa, M. Kubo, J. Phys. Chem. C 117 (2013) 15602.
[68] R. Messier, J. Nanophot. 2 (2008) 021995.
[69] J.A. Thornton, J. Vac. Sci. Technol. A 4 (1986) 3059.
[70] R.J. Zambrano, R.A.C.M.M. van Swaaij, M.C.M. van de Sanden, MRS Proc. 989 (2007), https://doi.org/10.1557/PROC-0989-A07-02, 0989–A07-02.
[71] Y.Y. He, Y.J. Su, M. Zhu, B.S. Cao, B. Dong, Sci. China-Phys. Mech. Astron 55 (2012) 2070.
[72] F.-A. Sarott, Z. Iqbal, S. Vepřek, Solid State Commun. 42 (1982) 465.